Extension of an empirical electron flux model from 6 to 20 Earth radii using CLUSTER/RAPID observations

M. H. Denton[1,2], M. G. G. T. Taylor[3], J. V. Rodriguez[4], and M. G. Henderson[5].

1. Center for Space Plasma Physics, Space Science Institute, CO 80301, USA.

2. New Mexico Consortium, Los Alamos, NM 87544, USA.

3. D/SCI, ESTEC, European Space Agency, 2201 AZ Noordwijk, The Netherlands

4. CIRES, University of Colorado at Boulder, CO 80305 USA.

5. ISR-1, Los Alamos National Laboratory, NM 87545, USA.

ABSTRACT

An existing empirical model of the electron fluxes at geosynchronous orbit (GEO) is extended radially outwards in the equatorial plane to ~6-20 Earth radii (R_E) using observations from the Research with Adaptive Particle Imaging Detectors (RAPID) instrument on the CLUSTER spacecraft. The new model provides electron flux predictions in the energy range ~45 eV to ~325 keV, as a function of local-time and radial distance from the Earth, with geomagnetic activity parameterised by the Kp index. The model outputs include the mean and median electron fluxes along with the standard deviation, and the 5th, 25th, 75th and 95th percentiles for the given input conditions. The flux outputs from the model are tested against in-sample observations from CLUSTER/RAPID, and out-of-sample observations from THEMIS/SST with good prediction efficiency during quiet and active intervals, as quantified by standard methods. This new model is intended to supplement current predictive capabilities in the magnetosphere for spacecraft operations, as well as providing the necessary boundary and/or input conditions for computational/physical models of the magnetospheric system when the necessary in-situ observations are unavailable. Whilst the new model can certainly not reproduce the rapid small-scale fluctuations inherent in spacecraft observations, it does provide a coarse capability to predict the flux of electrons close to the equatorial plane, based on radial distance, energy, local time, and geomagnetic activity, in regions where no in-situ assets are available.

1. Introduction

When forecasting the flux environment in the magnetosphere, one of two approaches is generally followed: (A) theoretical *physical modelling* of the magnetosphere is carried out, based on currently understood physical laws, whereby equations are solved computationally to provide flux estimates for the users. Such an approach is usually regarded as best practice for complete physical understanding, although it can be computationally expensive and relies on a well-developed understanding of the system being modeled (e.g. *Fok et al. [1999]*; *Jordanova et al.* [1997; 2003; 2018], *Lyon et al.*]2004]; *Zaharia et al.* [2005, 2006]; *Tóth et al.* [2005]; *Liemohn et al.* [2006]); (B) *empirical modelling* of the magnetosphere is carried out, whereby previously measured values of the flux under various conditions are used to make predictions of what the future fluxes will be under similar conditions. This approach relies on having extensive measurements of previous observations, under all necessary conditions, in order to accurately predict future fluxes. Given the vast databases of flux observations in the magnetosphere that are now available, this study utilizes the latter approach to extend a previously implemented empirical model.

The majority of military, operational and communication satellites operate in the inner magnetosphere, either at geosynchronous orbit (GEO) at 6.6 R_E (Earth radii), or closer to the Earth, and efforts to predict the electron and ion fluxes in this inner-magnetosphere region have received most effort to date (e.g. *Thomsen et al.* [2007]; *O'Brien* [2007]; *Sicard-Piet et al.* [2008]; *O'Brien and Lemon* [2009]; *Hartley et al.* [2014]; *Ganushkina et al.* [2013; 2014; 2015]; *Boynton et al.* [2013]; *Ginet et al.* [2014]; *Sillanpää et al.*[2017]; *Coleman et al.* [2018]). The perceived "priority mismatch" between the operational and scientific communities is also worthy of note [*O'Brien et al*., 2013]. Further from GEO satellites are primarily deployed for scientific exploration in the outer magnetosphere and solar-wind. However, the need for accurate predictions in these regions still exists. During the early space age, observations in the outer magnetosphere were sparse. However, over the past few decades there have been several long-term missions that have greatly extended the amount of data gathered throughout the outer magnetosphere (e.g. CLUSTER, THEMIS, GEOTAIL, MMS, etc). Models of the different regions sampled have been constructed using some of these data, for example the ion temperature, density, and pressure of the central plasma sheet [*Tsyganenko and Mukai*, 2003]. In the current study we utilize electron observations from Imaging Electron Spectrometer detector (IES) that forms part of the Research with Adaptive Particle Imaging Detectors (RAPID) instrument on the CLUSTER spacecraft [*Wilken et al.,* 1997; 2001; *Daly and Kronberg*, 2018; *Daly*, 2018] to extend empirical models of ion and electron fluxes at GEO [*Denton et al.*, 2015; 2016]. These previous models, based on data from the LANL satellites, cover ion and electron energies from ~1 eV to ~40 keV. In the current study, we use the same empirical modelling framework to develop flux predictions in the region radially outwards from GEO between ~6 and 20 R_E, close to the geomagnetic equator.

The new model is described in detail below. Comparisons are presented showing model predictions alongside in-situ data from a variety of sources. Goodness-of-fit calculations between the model fluxes and the observations are also presented. Finally, we discuss future work plans for possible improvements in empirical modeling and further extensions of the other models in both the inner and outer magnetosphere.

2. Data and Model Description

Our previously developed models (based on data from Los Alamos National Laboratory satellites) provide users with predictions of the ion and/or electron fluxes at GEO for any magnetic local time

(MLT), any energy (from ~1 eV to ~40 keV), and any activity, parameterized by either Kp or $-v_{sw}B_z$ [*Denton et al.*, 2015; 2016]. In the latter case, true forecasting of the fluxes is possible based on the upstream solar wind conditions (e.g. from the ACE or DSCOVR satellites), with a lead time of ~1 hour. The mean, median, and standard deviation in each model-bin are calculated, while bi-linear interpolation allows flux predictions to be made for any chosen input values. Both models return predictions of the 5th, 25th, 75th, and 95th percentiles of the flux values for any chosen combination of input values. In the $-v_{sw}B_z$ version of the model, the data are binned according to the prevailing upstream solar wind electric field ($-v_{sw}B_z$), rather than the Kp index, and for this version tri-linear interpolation is required to provide the flux forecasts. Due to the smaller database of CLUSTER/RAPID measurements, particularly during highly disturbed periods, the Kp index (a discrete variable) is used for the new flux model, rather than $-v_{sw}B_z$.

Earlier in the mission, data from the Cluster Ion Spectrometry (CIS) instrument (~5-32000 eV/q) were used to derive averaged ion parameters in the magnetosphere, [*Denton and Taylor*, 2008] and GPS observations were also used to infer electron properties in this region [*Denton and Cayton*, 2011]. The current study, and the model development, has evolved, in a somewhat convoluted manner, from those previous efforts.

The original models were coded in FORTRAN 77 (F77) although F90 and Python versions of the models have also been developed. Testing of these models has been carried out against out-of-sample observations by AMC-12 [*Denton et al.*, 2015; 2016]. During both calm and disturbed periods a good match is found between data and observations when quantified by either Root-Mean-Squared-Deviation (RMSD) or Normalized Root-Mean-Squared-Deviation (NRMSD). These metrics have previously been used to assess flux model performance in comparison with data (e.g. *Ganushkina et al.* [2013; 2014; 2015]; *Liemohn et al.* [2018]. See also *Legates and McCabe Jr.* [1999]). Our previously constructed -$v_{sw}B_z$ model has the ability to make true forecasts of the expected flux (if the upstream value of the -$v_{sw}B_z$ parameter is known). However, when compared with measured fluxes the performance of the Kp version of the model compared with the -$v_{sw}B_z$ version of the model (as quantified by RMSD and NRMSD values) is quite similar.

One limitation of these current models is that they only output flux predictions at GEO. The new model introduced below is a first attempt to extend the current models radially outwards from GEO and is based on electron observations made by the C4 (Tango) spacecraft during the years 2001-2016, inclusive. The CLUSTER/RAPID/IES omnidirectional flux data (using calibration file RAP_IES_C4_V332.CAL) were downloaded directly from the Cluster Science Archive in March 2018,. These data take into account the decay/degradation of the IES dectector response with time as detailed in full in *Kronberg et al.* [2018] and *Daly* [2018]. Additionally, it has been shown that in the inner magnetosphere, there is contamination of the RAPID/IES fluxes due to energetic electrons and ions present in the radiation belts and ring current [*Kronberg et al.* 2016; 2018]. This contamination varies with radial location and affects all energy channels, although in the region L*=6-9, the contamination is greatest in the top three energy channels and is dominated by >400 keV electrons. Over L*=6-9 and the top three energy channels, the simulated contamination level ranges from 4.9% to 34.55% (using mean fluxes from the AE9/AP9 models) [*Kronberg et al.*, 2016, Table 2]. The flux data used in the model have not been corrected for contamination; users should be aware of the contamination issue above 95 keV and refer to *Kronberg et al.* [2016] for further insight into the problem. One further issue affects the fluxes from RAPID/IES, namely a very low non-zero background (well-below the one-count-per-second level), that is likely due to solar-cycle modulated cosmic rays and has been quantified in detail by *Kronberg et al.* [2018] (see also *Smirnov et al.* [2019]). It was decided not to subtract these low background values from the fluxes prior to inclusion in the model. This decision was made based on the primary area of interest for the model being the magnetosphere, rather than regions beyond the magnetosphere, in the solar wind, where the background flux values are more of an issue. The model data grid itself (see Figure 3) does not specify regions inside or outside the magnetosphere, being based on spatial location only, and hence flux measurements from the solar wind, and the magnetosphere can both be present in a single bin. (Note: Model users concerned with the low flux values present in the solar wind, where background noise levels may be important, are referred directly to detailed work of *Kronberg et al.* [2018] on this topic).

In order to avoid complications in measuring and fully quantifying the pitch-angle distribution of the electrons along a particular magnetic field line, this initial version of an outer magnetosphere flux model only covers the region close to the GSM-xy plane (specifically where GSM-z values are restricted to ±2 R_E.). In the inner magnetosphere, this plane corresponds well with the location of the neutral current sheet, although at greater radial distances from the Earth there can be large differences between the current sheet location and the GSM-xy plane.

Figure 1 is a plot of example omnidirectional fluxes measured by CLUSTER/RAPID from 8th August 2002 to 26th September 2002. Due to the highly elliptical orbit, CLUSTER repeatedly cuts through the GSM-xy plane (and the location of this intercept migrated as the mission orbit evolved). Here, every 100th data point is plotted along the orbit for all spatial locations, however, only data from 6-20 R_E and from GSM-z ±2 are included in the model. This spatial region was chosen to avoid high levels of contamination of the data in the region due to the radiation belts, but also to provide overlap between this new model and our previous models that are valid at GEO (6.6 R_E). Figure 2 contains plots of the flux distribution values for each of the six energy ranges of the RAPID instrument (the approximate energy bins are 39.2-50.5, 50.5-68.1, 68.1-94.5, 94.5-127.5, 127.5-244.1, and 244.1-406.5 keV, with approximate centroid energies of 45, 59, 81, 110, 185, and 325 keV). In total, more than 3 million individual data points (from 2001 to 2016, inclusive) are used in the construction of the new model.

Following the same model framework as introduced in *Denton et al.* [2015], in the current study all available RAPID observations are binned into one of 14 bins in radial distance from 6 to 20 R_E (each bin covers 1 R_E in radial distance), into one of 24 bins in local time (each bin covers 1 hour), and into one of the six energy bins from ~40 to 406 keV. This binning used here is carried out for six discrete values of the Kp index [*Bartels et al.*, 1939; *Thomsen,* 2004]. The Kp bins used are: $0_0 \leq Kp < 1_0$, $1_0 \leq Kp < 2_0$, $2_0 \leq Kp < 3_0$, $3_0 \leq Kp < 4_0$, $4_0 \leq Kp < 5_0$, and $Kp \geq 5_0$ (<u>note</u>: sparse flux data for Kp values >5 necessitate the use of only six bins of Kp). Following the binning, the mean, median, and standard deviation of the values in each bin are calculated along with the 5th, 25th, 75th and 9th percentiles of all values. The resulting data-grid is a four-dimensional array (a tesseract) of each of these seven quantities. Figure 3 contains example plots of the mean flux in each bin at an energy of 185 keV for the six Kp bins listed above. The total number of data points contributing to each plot is also listed (with example count plots provided as supplementary material). In regions beyond ~18 R_E there are far fewer counts contributing to the model fluxes and these regions should be treated with caution.

The general morphology of the electrons in these plots is that the flux is greatest close to 6 R_E (i.e. near the outer edge of the electron radiation belt), and greater on the nightside than on the dayside. Dayside fluxes beyond ~10 R_E largely represent sampling in the solar-wind plasma. Previous work by *Åsnes et al.* [2008] defined identification criteria for particular regions in the magnetosphere (for ions) based on in-situ values of ion parameters such as plasma β_i and ion pressure, P_i. Here, the intention is not specifically to separate out different regions in any spatial location. Rather, the aim is to quantify the flux to be encountered by a satellite, regardless of which region it is situated within, and based on the prevailing conditions, parameterized (solely in this model) by the Kp index.

Figure 4 contains further example plots of the mean electron flux for the Kp range $2_0 \leq Kp < 3_0$ at all six energies listed above. The total number of data points contributing to each plot is also provided. As in Figure 3, the fluxes shown here are greatest on the nightside of the Earth, and diminish with increasing distance. Clearly, there is some inherent scatter between adjacent bins in the values shown in Figures 3 and 4. In order to provide model flux values in bins without any data, and also to avoid sharp jumps in the flux values between each bin, we carry out limited interpolation and smoothing on these data. The flux values plotted in Figure 5 are the same as those in Figure 4, but have been subjected to bi-linear interpolation in radial distance and local time, and also smoothed using a box-car average over three bins in local time and radial distance (cf. *Denton et al.* [2018]). The caveat remains that in regions beyond ~18 R_E there are far fewer counts contributing to the model fluxes and these regions should be treated with caution.

3. Comparison of Model Predictions with Observations

In order to compute a goodness-of-fit parameter for the model flux predictions, when compared to the actual observations, we follow previous practice [*Legates and McCabe Jr.*, 1999; *Ganushkina et al.*, 2015; *Denton et al.*, 2016] and utilize: (i) root-mean-squared deviation (RMSD), and (ii) normalized root-mean-squared deviation (NRMSD). Specifically,

$$\mathrm{NRMSD} = \mathrm{RMSD}\Big/(\overline{x}) = \sqrt{\frac{\sum_{x=1}^{n}\left[\left(x_{i,\,\mathrm{model}} - x_{i,\,\mathrm{measured}}\right)^2\right]}{n}}\Bigg/\left(\overline{x}\right) \qquad (1)$$

where n is the number of data points over the range of the comparison and $\overline{x}$ is the mean value of the parameter x during a specified interval (x=$\log_{10}$[flux] in this case). A value of zero for either of these parameters would indicate the predictions are a perfect match to the observations during the interval under consideration. NRMSD values <1 are generally considered to indicate a reasonable match between model and data.

3.1 Comparison with in-sample CLUSTER/RAPID observations

A comparison of model predictions with CLUSTER/RAPID fluxes is a so-called *in-sample* comparison, since the CLUSTER/RAPID fluxes themselves contributed to the flux model in the first place. However, such a comparison is still a useful check on the temporal and spatial accuracy of the model, and its integrity, under a variety of conditions. Figure 6 shows a comparison of the model predictions and the observations from CLUSTER/RAPID, with the fluxes plotted as a function of day-of-year (DOY) during a 20-day period in 2004. The mean flux prediction from the model is shown in blue with the observed data plotted in red (for clarity, the percentiles of the model flux are omitted). The Kp index is also shown, along with RMSD and NRMSD values computed for this interval. During this period the CLUSTER orbit apogee was around 18 R_E close to local midnight and the spacecraft repeatedly cut through the GSM-xy plane once every ~48 hours. Since the model is only applicable close to this plane, the data and model predictions are only shown in this region (GSM-z < ±2). The Kp index varied considerably during this period as a high-speed solar-wind stream (HSS) passed by the magnetosphere (e.g. *Denton et al.* [2006]; *McPherron and Weygand*, [2006]; *Borovsky and Denton* [2006]). However, the model flux predictions are generally well-aligned with the actual observations (NRMSD<0.5), although it is clear that they fluctuate considerably less than the observed data values. This is unsurprising given that the model values are dependent only upon Kp, local time, and radial distance from the Earth, and these parameters change very slowly. The model values at the highest Kp values are somewhat lower than observed but otherwise fall somewhere in the middle of the observed fluxes throughout this interval.

Figure 7 contains plots of the data and model fluxes from DOY 258, at a higher time resolution, and at multiple energies, but in a similar format as in Figure 6. Here, the model flux predictions (blue) are again plotted alongside the observed fluxes (red). The mean, median, and percentiles are all plotted to demonstrate the range of model flux prediction values during this period. The small-scale fluctuations in the CLUSTER/RAPID flux observations during this pass through the equatorial plane are now much more evident. The model values are inherently smooth due to the 3-hour cadence of the Kp index and cannot represent the small-scale temporal and/or spatial fluctuations in the flux that are measured by RAPID. At all six energies the model predictions show only small variations, although as indicated by the RMSD and NRMSD values, they are generally reasonably well-aligned in absolute magnitude to the observations. Other in-sample comparisons carried out show similar model-data agreement during quiet and active periods.

3.2 Comparison with out-of-sample THEMIS/SST observations

As in the evaluation of previous models, in addition to in-sample testing, it is also necessary to perform a 'real-world' test with data that are not incorporated with the actual model construction itself. Here, this out-of-sample testing is carried out with in-situ flux observations from the Solid State Telescope (SST) carried on board the THEMIS-C spacecraft. The SST instrument measures electrons in the range >30 keV to >300 keV [*Angelopoulos*, 2008; *Angelopoulos et al.*, 2008] and here the fluxes are examined during an active period in 2008. At this time the orbit of THEMIS-C was aligned for studies of the magnetotail with an apogee in the pre-midnight sector, within the spatial domain of the model.

<u>Note</u>: Previous work identified offsets between measured electron fluxes from the THEMIS/SST and the Synchronous Orbit Particle Analyzer (SOPA) onboard the LANL-01A satellite [*Ni et al.*, 2011]. That study concluded "*Compared to the LANL-01A SOPA data, the THEMIS SST data underestimate the electron fluxes within a factor of 2 for the 40–140 keV energy channels and overestimate the electron fluxes within a factor of 3 for the 204–2159 keV energy channels*". Given the SST data used here are simply for large-scale model verification, no inter-calibration or cross-calibration between THEMIS/SST, LANL/SOPA, and/or the CLUSTER/RAPID electron fluxes has been attempted.

Figure 8 shows example electron fluxes at ~142 keV (Level 2) measured by THEMIS/SST during a 6-day period in 2008. This reasonably active period encompasses the passage of a HSS past the magnetosphere, with Kp varying from ~0 to 6-. The SST electron flux during this interval is plotted along with model predictions, in the same format as Figure 6 (red=data, blue=model, purple=Kp index). Median and percentile values are again omitted for clarity. The THEMIS-C orbit in 2008 was close to the equatorial plane and hence, there is a higher proportion of fluxes measured within the model domain (~6-20 R_E and ±2 GSM-z) than for the CLUSTER satellite. It is also worth noting that in contrast to the CLUSTER satellite, THEMIS orbits rapidly in radial distance and local-time, whilst the CLUSTER orbit cut through the equatorial plane repeatedly, at a roughly constant spatial position and fixed local time. During the interval plotted in Figure 8 the model fluxes track the large-scale variations observed by THEMIS/SST very well, during both quite and active phases of the HSS, (RMSD~0.94, NRMSD~0.2), with the absolute magnitude of the flux well-aligned between model and data. The model does not capture the small-scale variations, but does capture the broad flux level at all points during this period.

Figure 9 contains a series of plots detailing the electron fluxes at four representative energies (53 keV, 96 keV, 142 keV, and 207 keV) during DOY 69-70 of the active interval shown in Figure 8. In this figure, the median and percentiles are also indicated by the dashed lines. During this interval the THEMIS orbital apogee was on the nightside in the post-dusk sector (~21 LT). The model again is well-aligned with the absolute magnitude of the electron flux at these four energies, although, similarly to the CLUSTER/RAPID comparison with the model fluxes in Section 3.1, here the model does not capture more rapid changes evident in the observations (that are likely due to small-scale spatial and/or temporal features). The RMSD and NRMSD values for the four energies plotted provide a quantified measure of the goodness-of-fit of model-to-data.

3.3 Comparison with original LANL/MPA flux model

As a final check of the model outputs, we perform a test comparison of the original Kp-based flux model at geosynchronous orbit with the new model in the same location. Figure 10 contains a summary of the results for $Kp=2_0$. In general the absolute fluxes for each model are in good agreement at GEO (the LANL flux model values fall within the inter-quartile range of the new CLUSTER model) except in the region centred on local midnight (20:00-04:00 MLT). Here, the CLUSTER/RAPID model fluxes are substantially lower than the model fluxes from LANL/MPA. No clear reason for this discrepency has been identified, except to state that there are significantly more individual observations in this region from LANL/MPA (seven satellites with almost two full solar-cycles of coverage), compared to CLUSTER/RAPID. Hence, at GEO, our general recommendation is to use the original model.

4. Discussion and Summary

Predicting the flux environment within the magnetosphere is of interest to the scientific and operational community. Accurate predictions help to confirm our understanding of the physics operating in the region, whilst also helping to develop, build, and maintain robust satellites and on-orbit measurement capabilities. Such predictions can follow either a theoretical or an empirical methodology and here we have utilized the latter. Whilst much effort to date has considered the region close to Earth (either at GEO, or inwards of GEO in the inner magnetosphere), the study described here has developed flux predictions further afield in the magnetosphere. Electron flux values are predicted using an empirical model, in the region from ~6-20 R_E, and provided to a user who inputs any permissible value of Kp, radial distance, local-time, and energy. The flux values returned to the user are, based on the model testing described above, a good match to the values actually measured on orbit by CLUSTER/RAPID and THEMIS/SST. Flux values on the nightside of the Earth, beyond GEO, are particularly useful from a predictions perspective since the plasma sheet material on the nightside is likely to be convected to the inner magnetosphere at some point in future, due to enhancements in the convective electric field [*Lavraud et al.* [2005, 2006]; *Denton et al.* [2007; 2009; 2017]).

However, there are many limitations to this newly developed model and these include: (i) the limited energy range; (ii) the lack of ion predictions; (iii) the lack of compositional information; (iv) the inability of the model to capture small spatial/temporal scale fluctuations observed in the in-situ data. Our intention is to address these issues by adding further data sources (particularly ion data) as time and availability permit.

The observed fluxes fluctuate much more rapidly than the three-hour time cadence of the Kp index, typically in response to dynamic changes in the solar wind that have timescales much less than one hour in duration [*King and Papitashvili*, 2005]; (v) the Kp index itself is calculated from the K index, and this is primarily based on magnetometer data taken at the Earth's surface. As a result, estimates of flux at Earth (geosynchronous orbit), based on the Kp index, are only available on an instantaneous basis (i.e. a 'nowcast'), rather than being true advance predictions (i.e. a 'forecast').

Despite these limitations, the flux model is a useful first step on which to build in future. Potential pathways to developing the model to address the above limitations include: (i) use of electron (and ion) fluxes measured by other instruments on CLUSTER or on other satellites (e.g. GOES, THEMIS, GEOTAIL, etc.); (ii) use of electron flux and ion flux and/or compositional information in the inner magnetosphere (e.g. from the Radiation Belt Storm Probes mission); (iii) ingesting more data into the model to decrease the spatial scale of the bins; (iv) cross-calibration of the fluxes between each satellite to improve overall compatibility of including data from different instruments/missions; (v) changing the activity index from Kp to $-v_{sw}B_z$ or to a physically-derived coupling function (e.g. *Newell et al.* [2007], *Borovsky* [2013, 2014], and *McPherron et al.*[2015]), if the abundance of data within the model makes this a possibility. This would improve temporal resolution of the model predictions and permit true forecasts to be made by driving the model direction with upstream solar-wind conditions. Such developments are planned in the future.

In summary:

1. A new model of the electron fluxes in the region from 6-20 R_E, close to the GSM-xy plane, has been developed. This model is parameterised by local time, radial distance from Earth, energy, and the Kp index.. The model provides estimates of the mean electron flux in this region, along with median, standard-deviation and the 5th, 25th, 75th, and 95th percentile fluxes.

2. Comparison of the flux model predictions with in-sample CLUSTER/RAPID electron fluxes and out-of-sample electron fluxes from THEMIS/SST demonstrates that the model reproduces the broad variations in electron flux actually observed in-situ, as determined by Root-Mean-Squared-Deviation (RMSD) and the Normalized Root-Mean-Squared Deviation (NRMSD). Small-scale temporal and/or spatial fluctuations in the data are not resolved.

3. Observed fluxes are generally found to be almost always within the 5th to 95th percentile envelope of the model predictions.

The model is freely available to users under the GNU General Public License v3.0 by contacting the author directly or via the model webpage at http://gemelli.spacescience.org/mdenton/.

Acknowledgements

The authors acknowledge the OMNI database for the solar wind and geophysical parameters used in this study. This work was primarily supported by the NASA Living With a Star (LWS) Grant:

80NSSC17K0682, as well as NASA grants NNX16AB75G and NNX16AB83G. All data from the CLUSTER mission are available via the Cluster Science Archive (https://www.cosmos.esa.int/web/csa) and we acknowledge the detailed work on calibration of the RAPID data carried out by the team. THEMIS data are available via the CDAWeb. We acknowledge D. Larson and the late R. P. Lin for use of SST data. The flux model introduced here (and other associated flux models), can be obtained from MHD at mdenton@spacescience.org or directly via http://gemelli.spacescience.org/mdenton/ . We also acknowledge the reviewer's comments and suggestions on our originally submitted manuscript that helped improve the final version of this study.

References

Angelopoulos, V., The THEMIS mission, Space Sci. Rev., 141, 5–34, doi:10.1007/s11214-008-9336-1, 2008.

Angelopoulos, V., et al., First results from the THEMIS mission, Space Sci. Rev., 141, 453–476, doi:10.1007/s11214-008-9378-4, 2008.

Åsnes, A., R.W.H. Friedel, B. Lavraud, G.D. Reeves, M.G.G.T. Taylor, and P. Daly, Statistical properties of tail plasma sheet electrons above 40 keV, J. Geophys. Res., 113, A03202, 2008.

Bartels, J., N. A. H. Heck, and H. F. Johnstone, The three-hour-range index measuring geomagnetic activity, J. Geophys. Res., 44, 411-454, 1939.

Borovsky, J. E., Canonical correlation analysis of the combined solar wind and geomagnetic index data sets, J. Geophys. Res. Space Physics, 119, 5364–5381, 2014.

Borovsky, J. E., Physical improvements to the solar wind reconnection control function for the Earth's magnetosphere, J. Geophys. Res. Space Physics, 118, 2113–2121, 2013.

Borovsky, J. E., and M. H. Denton, Differences between CME-driven storms and CIR-driven storms, J. Geophys. Res., 111, A07S08, doi:10.1029/2005JA011447, 2006.

Boynton, R., et al., The analysis of electron fluxes at geosynchronous orbit employing a Narmax approach. J. Geophys. Res., 118, 1500–1513, 2013.

Coleman, T., McCollough, J. P., Young, S., & Rigler, E. J., Operational nowcasting of electron flux levels in the outer zone of Earth's radiation belt, Space Weather, 16, 501–518, 2018.

Daly, P. W., Cluster Science Archive: Interface Control Document for RAPID. Tech. Rep. CAA-EST-ICD-0001, V6.0, European Space Agency, Paris, 2018.

Daly, P. W., and E. A. Kronberg, User guide to the RAPID measurements in the Cluster science archive (CSA): Version 5.2, Tech. Rep. CAA-EST-UG-RAP, European Space Agency, Paris, 2018.

Denton, M. H., and T. E. Cayton, Density and temperature of energetic electrons in the Earth's magnetotail derived from high-latitude GPS observations during the declining phase of the solar cycle, Ann. Geophys., 29, 1755, doi:10.5194/angeo-29-1755-2011, 2011.

Denton, M. H., and M. G. G. T. Taylor, Solar wind dependence of ion parameters in the Earth's magnetospheric region calculated from CLUSTER observations, Ann. Geophys., 26, 387-394, 2008 (SRef-ID: 1432-0576/angeo/2008-26-387), 2008.

Denton, M. H., R. Kivi, T. Ulich, C. J. Rodger, M. A. Clilverd, R. B. Horne, and A. J. Kavanagh, Solar proton events and stratospheric ozone depletion over northern Finland, J. Atmos. Sol-Terr. Phys., doi:10.1016/j.jastp.2017.07.003, 177, 218-227, 2018.

Denton, M. H., G. D. Reeves, B. A. Larsen, R. F. W. Friedel, M. F. Thomsen, P. A. Fernandes, R. M. Skoug, H. O. Funsten, and L. K. Sarno-Smith, On the origin of low-energy electrons in the inner magnetosphere: Fluxes and pitch-angle distributions, J. Geophys. Res. Space Physics, 122, 1789–1802, doi:10.1002/2016JA023648, 2017.

Denton, M. H., M. G. Henderson, V. K. Jordanova, M. F. Thomsen, J. E. Borovsky, J. Woodroffe, D. P. Hartley, and D. Pitchford, An improved empirical model of electron and ion fluxes at geosynchronous orbit based on upstream solar wind conditions, Space Weather, 14, 511–523, doi:10.1002/2016SW001409, 2016

Denton, M. H., M. F. Thomsen, V. K. Jordanova, M. G. Henderson, J. E. Borovsky, J. S. Denton, D. Pitchford, and D. P. Hartley, An empirical model of electron and ion fluxes derived from observations at geosynchronous orbit, Space Weather, 13, 2015.

Denton, M. H., and J. E. Borovksy, The superdense plasma sheet in the magnetosphere during high-speed-stream-driven storms: Plasma transport timescales. J. Atmos. Sol-Terr. Phys, 71, 1045-1058, 2009

Denton, M. H., M. F. Thomsen, B. Lavraud, M. G. Henderson, R. M. Skoug, H. O. Funsten, J.-M. Jahn, C. J. Pollock, and J. M. Weygand, Transport of plasma sheet material to the inner magnetosphere, Geophys. Res. Lett., 34, L04105, doi:10.1029/2006GL027886, 2007.

Borovsky, J. E., and M. H. Denton, The differences between CME-driven storms and CIR-driven storms, J. Geophys. Res., 111, A07S08, doi:10.1029/2005JA011447.Denton et al., 2006.

Fok, M.-C., Moore, T. E., and Delcourt, D. C.: Modelling of inner plasma sheet and ring current during substorms, J. Geophys. Res., 104, 14 557–14 569, 1999.

Ganushkina, N. Y., O. A. Amariutei, D. Welling, and D. Heynderickx, Nowcast model for low-energy electrons in the inner magnetosphere, Space Weather, 13, 16–34, doi:10.1002/2014SW001098, 2015.

Ganushkina, N. Y., M. W. Liemohn, O. A. Amariutei, and D. Pitchford, Low-energy electrons (5–50 keV) in the inner magnetosphere, J. Geophys. Res. Space Physics, 119, 246–259, doi:10.1002/2013JA019304, 2014.

Ganushkina, N. Y., O. Amariutei, Y. Y. Shpritz, and M. Liemohn, Transport of the plasma sheet electrons to the geostationary distances, J. Geophys. Res. Space Physics, 118, 82–98, doi:10.1029/2012JA017923, 2013.

Ginet, G. P., T. P. O'Brien, S. L. Huston, W. R. Johnston, T. B. Guild, R. Friedel, C. D. Lindstrom, C. J. Roth, P. Whelan, R. A. Quinn, D. Madden, S. Morley, and Yi-Jiun Su, AE9, AP9 and SPM: New Models for Specifying the Trapped Energetic Particle and Space Plasma Environment, in The Van Allen Probes mission, eds N. Fox and J. L. Burch, Springer, doi:10.1007/978-1-4899-7433-4, ISBN: 978-1-4899-7432-7, 2014.

Hartley, D. P., M. H. Denton, and J. V. Rodriguez, Electron number density, temperature, and energy density at GEO and links to the solar wind: A simple predictive capability, J. Geophys. Res. Space Physics, 119, 4556–4571, doi:10.1002/2014JA019779, 2014.

V. K. Jordanova, G. L. Delzanno, M. G. Henderson, H. C. Godinez, C. A. Jeffery, E. C. Lawrence, S. K. Morley, J. D. Moulton, L. J. Vernon, J. R. Woodroffe, T. V. Brito, M. A. Engel, C. S. Meierbachtol, D. Svyatsky, Y. Yu, G. Tóth, D. T. Welling, Y. Chen, J. Haiducek, S. Markidis, J. M. Albert, J. Birn, M. H. Denton, R. B. Horne, Specification of the near-Earth space environment with SHIELDS, J. Atmos. Sol-Terr. Phys., Volume 177, 1148-159, 2018.

Jordanova., V. K., Kozyra, J. U., Nagy, A. F., and Khazanov, G. V., Kinetic model of ring current-atmosphere interactions, J. Geophys. Res., 102, 14 279–14 291, 1997.

King, J. H., and N. E. Papitashvili, Solar wind spatial scales in and comparisons of hourly Wind and ACE plasma and magnetic field data, J. Geophys. Res., 110, A02104, 2005.

Kronberg, E. A., M. V. Rashev, P. W. Daly, Y. Y. Shprits, D. L. Turner, A. Drozdov, M. Dobynde, A. C. Kellerman, T. A. Fritz, V. Pierrard, K. Borremans, B. Klecker, and R. Friedel, Contamination in electron observations of the silicon detector on board Cluster/RAPID/IES/instrument in Earth's radiation belts and ring current, Space Weather, 14, 449-462, 2016.

Kronberg, E. A., P. W. Daly, and E. Vilenius, Calibration report of the RAPID measurements in the Cluster science archive (CSA): Version 5.1, Tech. Rep. CAA-EST-CR-RAP, European Space Agency, Paris, 2018.

Lavraud, B., M. F. Thomsen, J. E. Borovsky, M. H. Denton, and T. I. Pulkkinen, Magnetosphere preconditioning under northward IMF: Evidence from the study of coronal mass ejection and corotating interaction region geoeffectiveness, J. Geophys. Res., 111, A09208, doi:10.1029/2005JA011566, 2006.

Lavraud, B., M. H. Denton, M. F. Thomsen, J. E. Borovsky, and R. H. W. Friedel, Superposed epoch analysis of dense plasma access to geosynchronous orbit, Ann. Geophys., 23, 2519–2529, 2005.

Legates, D. R., and G. J. McCabe Jr., Evaluating the use of “goodness-of-fit” Measures in hydrologic and hydroclimatic model validation, Water Resour. Res., 35(1), 233–241, doi:10.1029/1998WR900018, 1999.

Liemohn, M. W., Ridley, A. J., Kozyra, J. U., Gallagher, D. L., Thomsen, M. F., Henderson, M. G., Denton, M. H., Brandt, P. C., and Goldstein, J.: Analyzing the electric field morphology through data-model comparisons of the Geospace Environment Modeling Inner Magnetosphere/Storm Assessment Challenge events, J. Geophys. Res., 111, A11S11, 2006.

Liemohn, M. W., et al., Model evaluation guidelines for geomagnetic index predictions. Space Weather, 16, 2079–2102, 2018.

Lyon, J. G., J. A. Fedder, and C. M. Mobarry, The Lyon-Fedder-Mobarry (LFM) Global MHD Magnetospheric Simulation Code, J. Atmos. Sol.-Terr. Phys., 66, Issue 15-16, 1333-1350, 2004.

McPherron, R. L., T.-S. Hsu, and X. Chu, An optimum solar wind coupling function for the AL index. J. Geophys. Res. Space Physics, 120, 2494–2515, doi: 10.1002/2014JA020619, 2015.

McPherron, R. L. and Weygand, J.: The solar wind and geomagnetic activity as a function of time relative to corotating interaction regions, in: Recurrent Magnetic Storms, edited by: Tsurutani, B., McPherron, R., Gonzalez, W., Lu, G., Sobral, J. H. A., and Gopalswamy, N., pg. 125, AGU, 2006.

Newell, P. T., T. Sotirelis, K. Liou, C.-I. Meng, and F. J. Rich, A nearly universal solar wind-magnetosphere coupling function inferred from 10 magnetospheric state variables, J. Geophys. Res., 112, A01206, doi:10.1029/2006JA012015, 2007.

Ni, B., Y. Shprits, M. Hartinger, V. Angelopoulos, X. Gu, and D. Larson, Analysis of radiation belt energetic electron phase space density using THEMIS SST measurements: Cross-satellite calibration and a case study, J. Geophys. Res.,116, A03208, 2011.

O'Brien, T. P., J. E. Mazur, and J. F. Fennell, The Priority Mismatch Between Space Science and Satellite Operations, Space Weather, 11, doi:10.1002/swe.20028, 2013.

O'Brien, T. P., SEAES-GEO: A spacecraft environmental anomalies expert system for geosynchronous orbit, Space Weather, 7, S09003, 2009.

O'Brien, T. P., and C. L. Lemon, Reanalysis of plasma measurements at geosynchronous orbit, Space Weather, 5, S03007, doi:10.1029/2006SW000279, 2007.

Sicard-Piet, A., S. Bourdarie, D. Boscher, R. H. W. Friedel, M. Thomsen, T. Goka, H. Matsumoto, and H. Koshiishi, A new international geostationary electron model: IGE-2006, from 1 keV to 5.2 MeV, Space Weather, 6, S07003, doi:10.1029/2007SW000368, 2008.

Sillanpää, I., N. Y. Ganushkina, S. Dubyagin, and J. V. Rodriguez, Electron fluxes at geostationary orbit fromGOES MAGED data, Space Weather, 15, doi:10.1002/2017SW001698, 2017.

Smirnov, A.G., E.A Kronberg, F. Latallerie, P.W. Daly, N. Aseev, Y.Y. Shprits, A. Kellerman, S. Kasahara, D. Turner, M.G.G.T. Taylor, Electron intensity measurements by the Cluster/RAPID/IES instrument in Earth's radiation belts and ring current, Space Weather, (in press) 2019.

Tóth, G., et al., Space Weather Modeling Framework: A new tool for the space science community, J. Geophys. Res., 110, A12226, doi:10.1029/2005JA011126, 2005.

Thomsen, M. F., Why Kp is such a good measure of magnetospheric convection, Space Weather, 2, S11004, doi:10.1029/2004SW000089, 2004.

Thomsen, M. F., M. H. Denton, B. Lavraud, and M. Bodeau, Statistics of plasma fluxes at geosynchronous orbit over more than a full solar cycle, Space Weather, 5, S03004, doi:10.1029/2006SW000257, 2007.

Tsyganenko, N. A. and Mukai, T. Tail plasma sheet models derived from Geotail particle data, J.

Geophys. Res., 108(A3), 1136, doi:10.1029/2002JA009707, 2003.

Wilken, B., et al., RAPID - The imaging energetic particle spectrometer on cluster, Space Sci. Rev., 79(1 – 2), 399 – 473, 1997.

Wilken, B., et al., First results from the RAPID imaging energetic particle spectrometer on board Cluster, Ann. Geophys., 10, 1355 – 1366, 2001.

Zaharia, S., M. F. Thomsen, J. Birn, M. H. Denton, V. K. Jordanova, and C. Z. Cheng, Effect of storm-time plasma pressure on the magnetic field in the inner magnetosphere, Geophys. Res. Lett., 32, L03102, doi:10.1029/2004GL021491, 2005.

Zaharia, S., V. K. Jordanova, M. F. Thomsen, and G. D. Reeves, Self-consistent modeling of magnetic fields and plasmas in the inner magnetosphere: Application to a geomagnetic storm, J. Geophys. Res., 111, A11S14, doi:10.1029/2006JA011619, 2006.

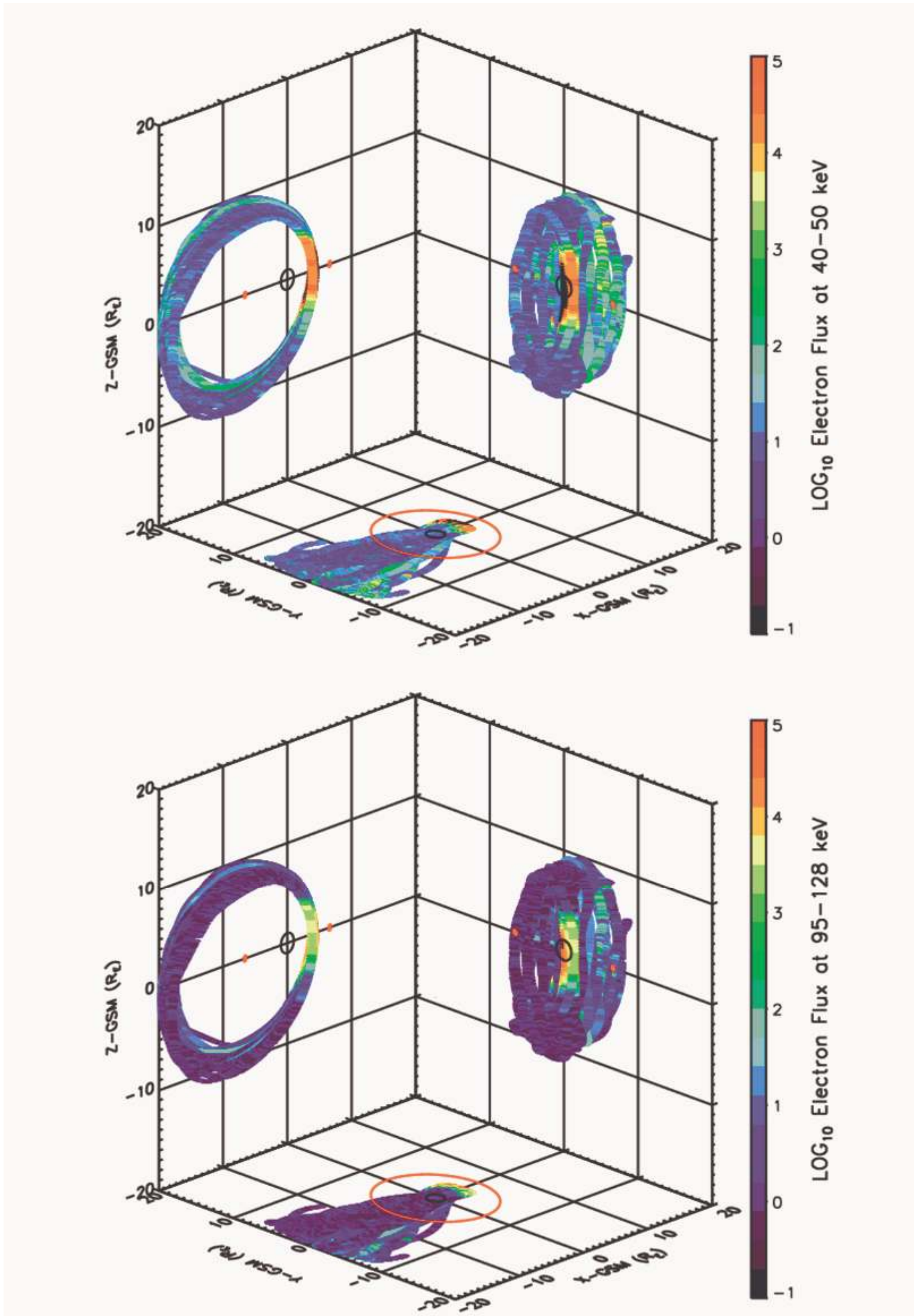

Figure 1. Example electron fluxes at two energies from CLUSTER/RAPID plotted in the GSM coordinate system during the period from 8th August 2002 to 26th September 2002. The apogee of the orbit, cutting through the xy-plane, was deep in the magnetotail on the nightside of the Earth during this period, Every 100th data point is plotted.

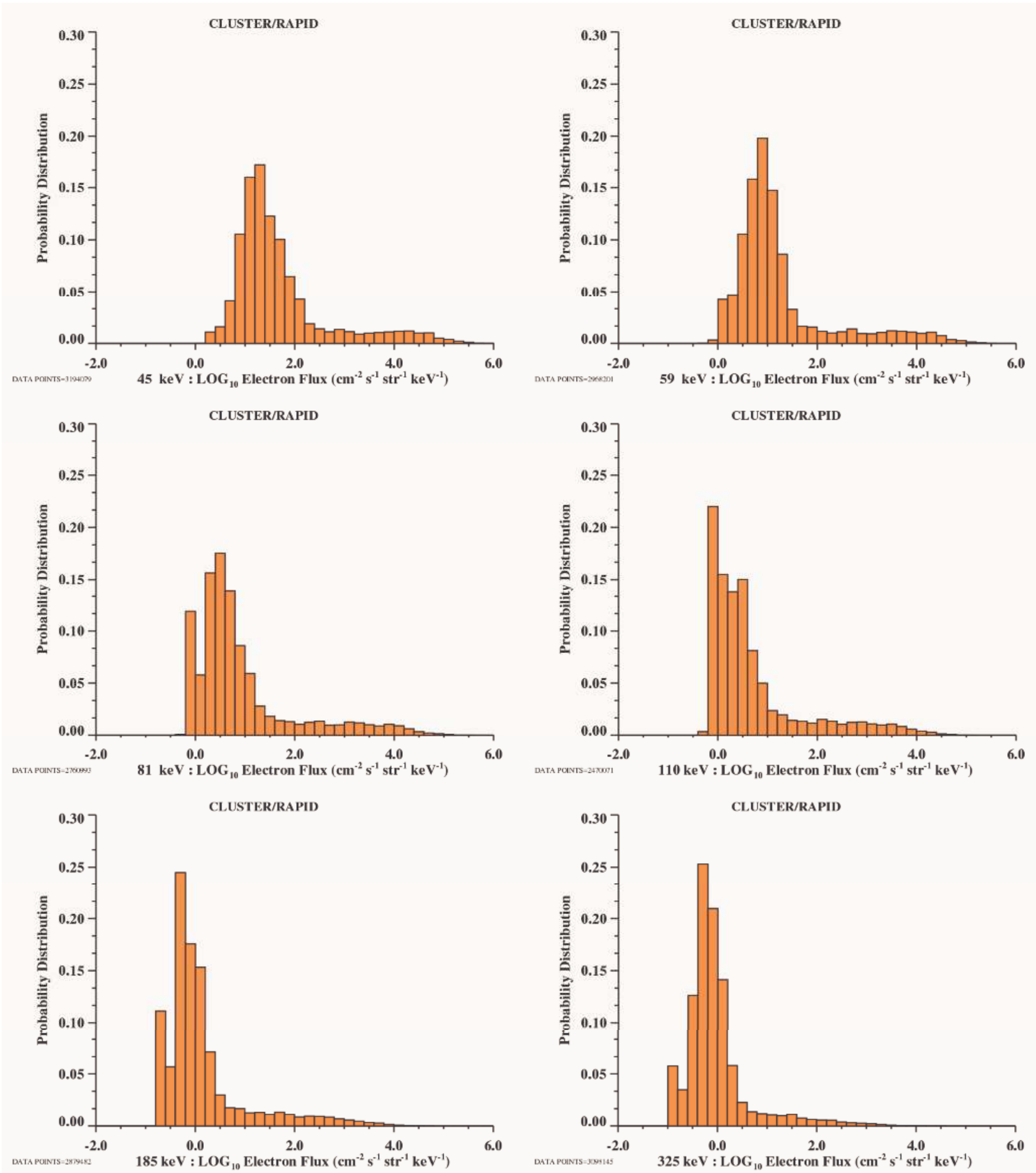

Figure 2. Flux probability distributions for the six energies of the CLUSTER/RAPID instrument. Only data within the model domain are included in these distributions. Each distribution has an extended tail, likely the region closest to the Earth (where the satellite spends the least amount of time during each orbit).

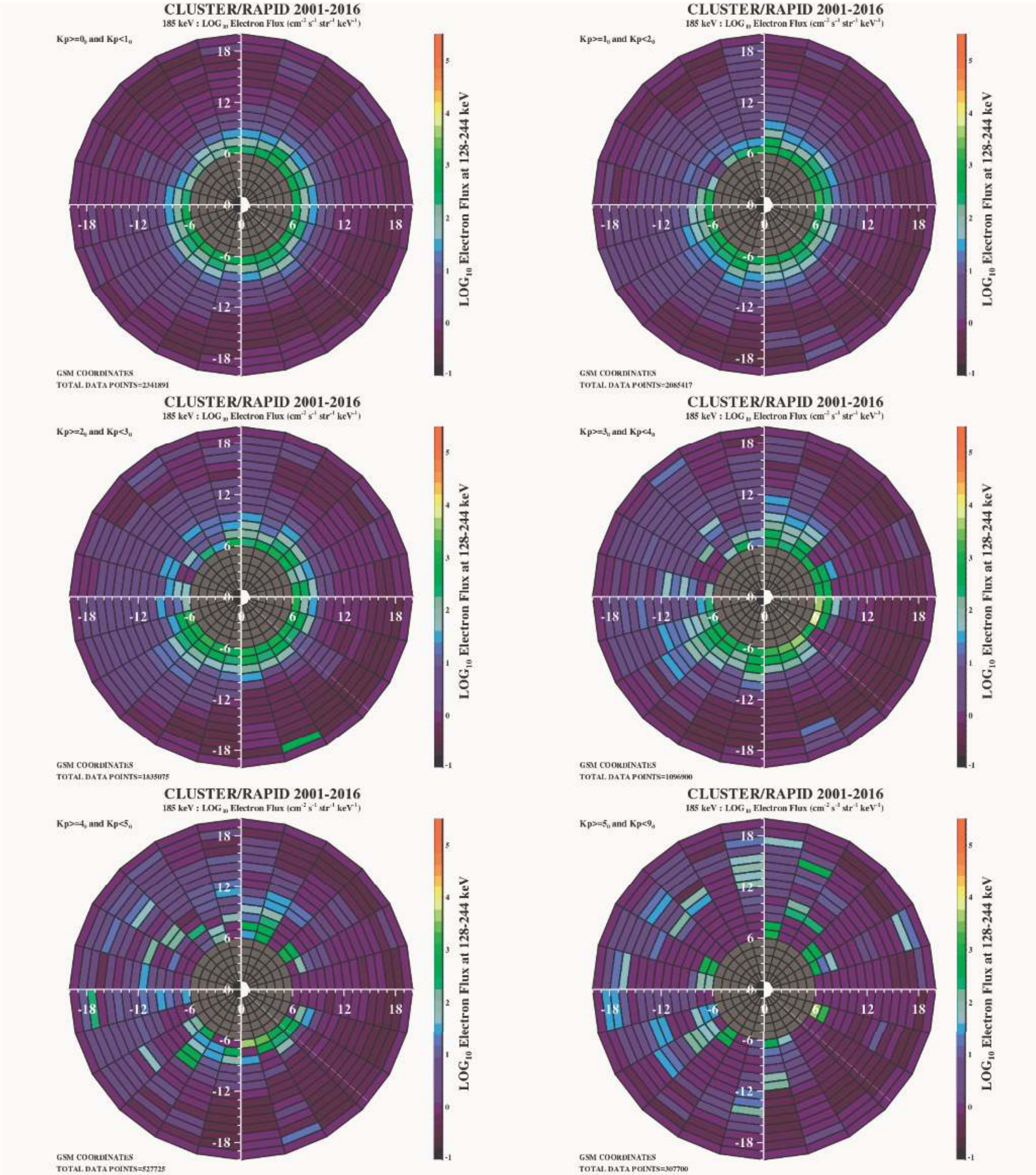

Figure 3. Schematic showing the binning scheme for the flux model in the GSM-xy plane. Six Kp ranges are shown, for the energy 185 keV. The total number of counts contributing to each plot is also given.

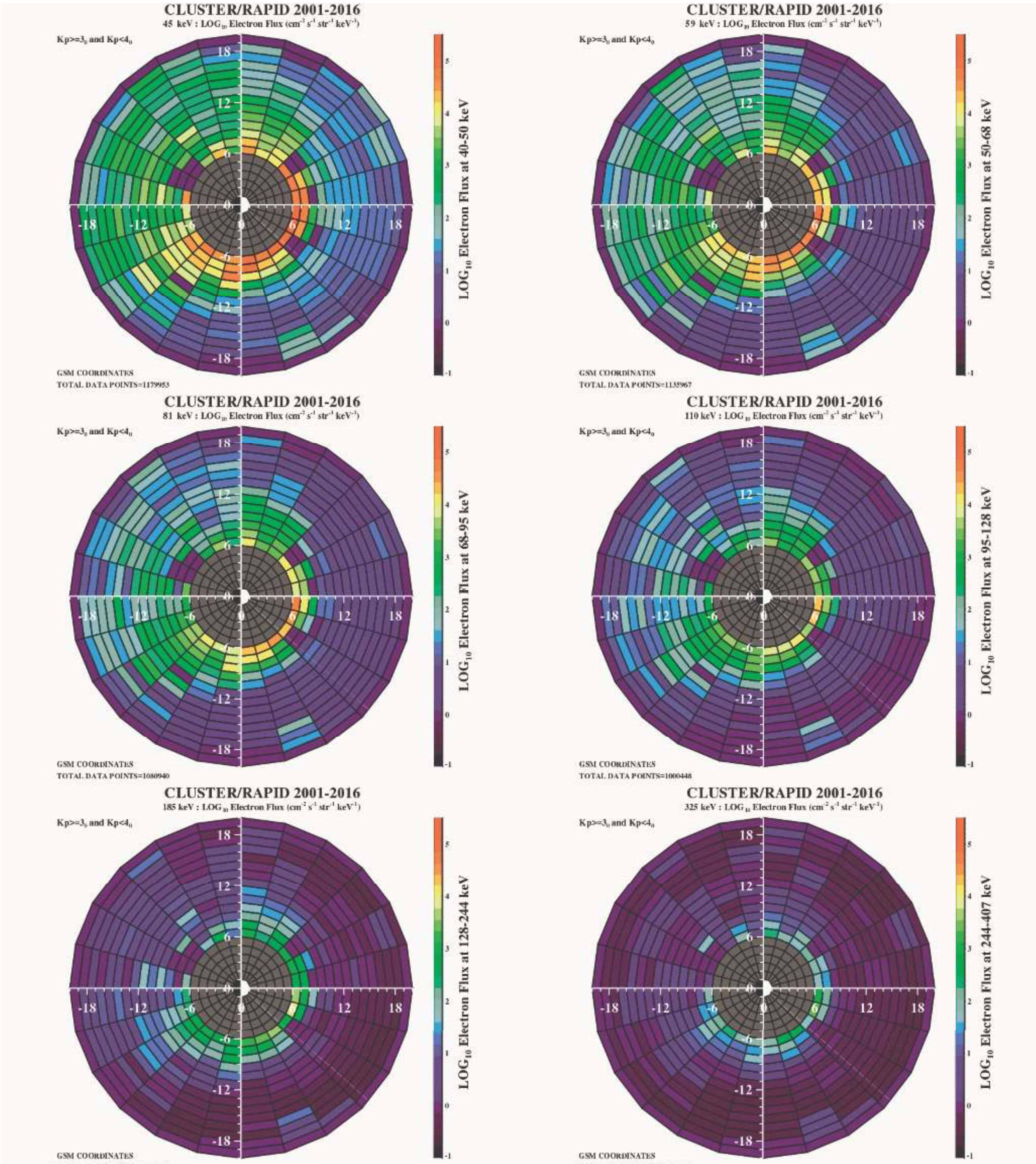

Figure 4. Schematic showing example plots of the mean flux in each bin in the GSM-xy plane. Six energy ranges are shown, for $2_0 \leq Kp < 3_0$. The total number of counts contributing to each plot is also given.

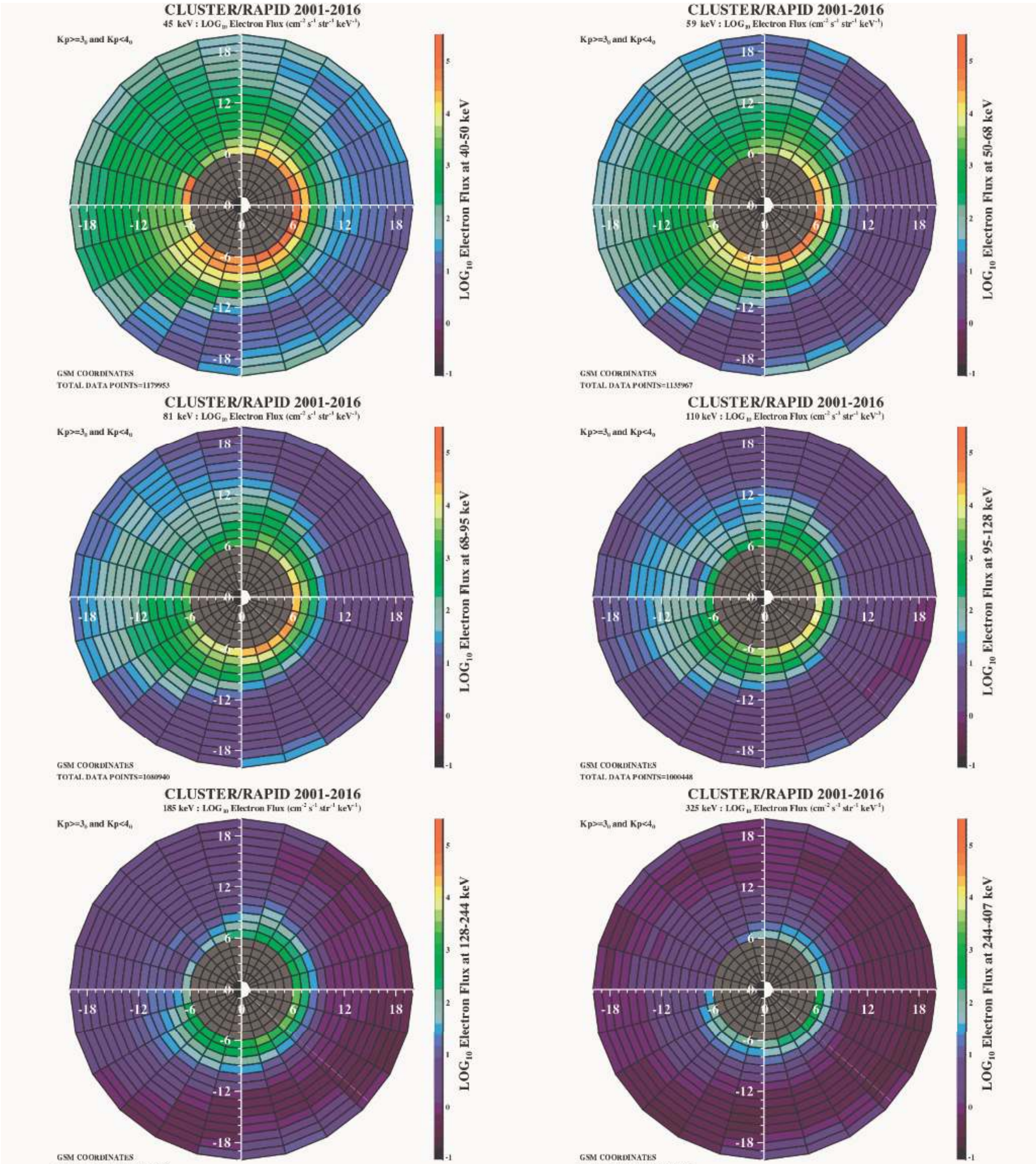

Figure 5. Same as Figure 3 but after the data have been interpolated and smoothed using a box-car average.

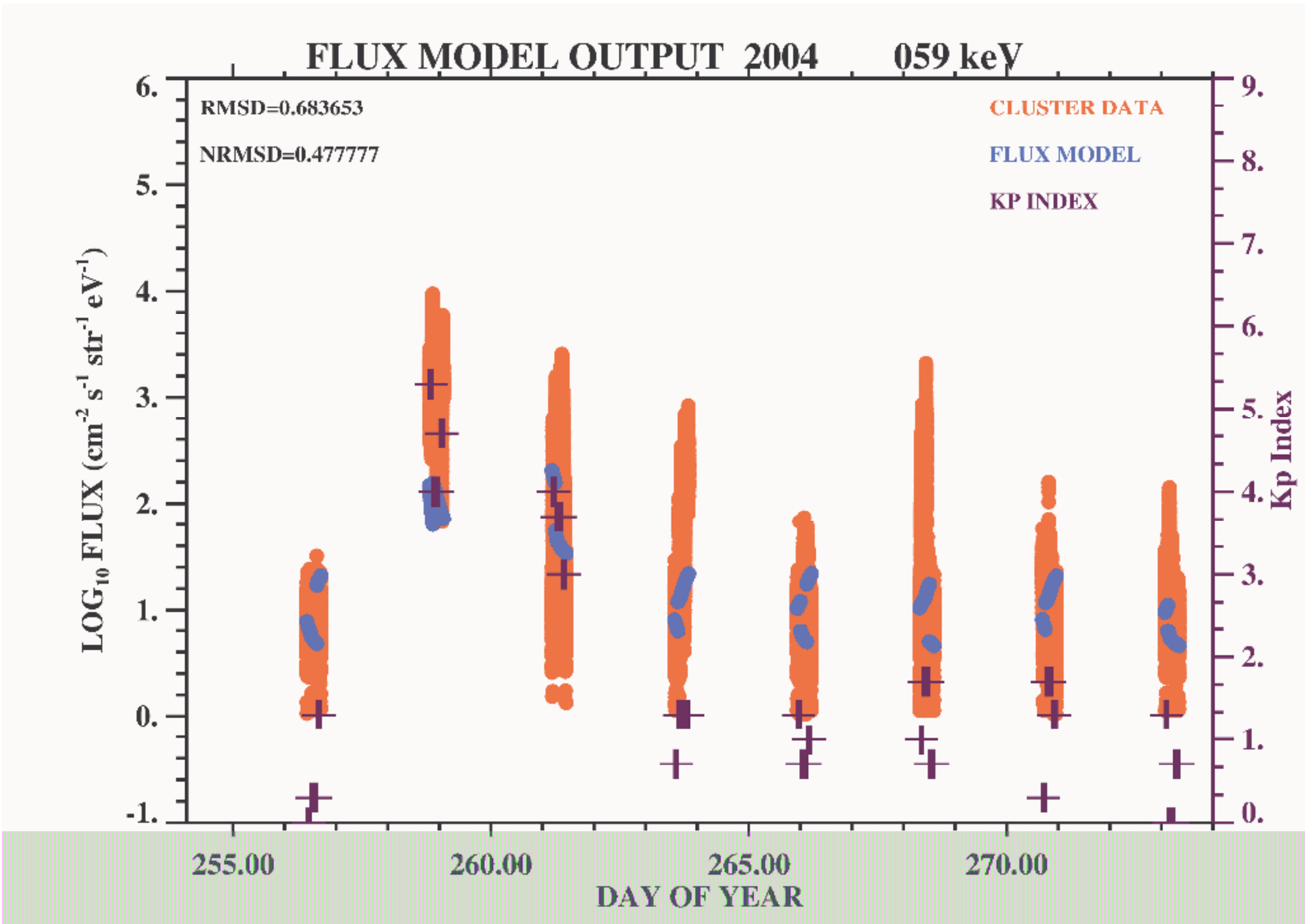

Figure 6. A comparison of electron observations by CLUSTER/RAPID at 59 keV (red) and model flux predictions (blue) during an active 20-day period in 2004. The Kp index is also shown (purple crosses). During this interval the CLUSTER orbit apogee was around 18 R_E and close to local midnight. Data are plotted in the region within ±2 R_E of GSM-z=0.

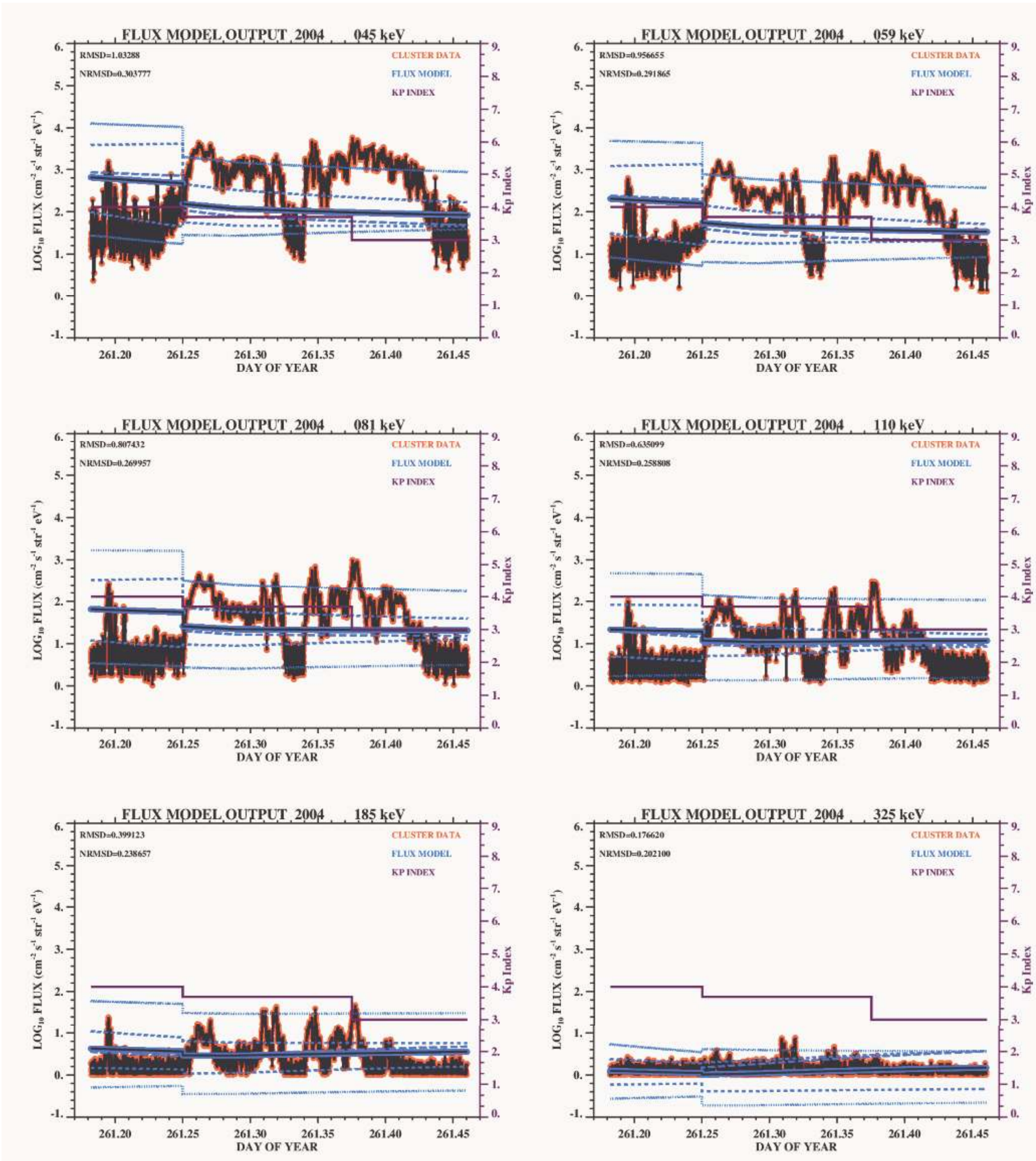

Figure 7. A detailed comparison of the observed electron fluxes (red/black) at six energies during day-of-year 258 (14th September) in 2004 with model flux predictions (blue). During this interval CLUSTER was cutting through the GSM-xy plane at a radial distance of ~18 R_E near local midnight. The mean flux prediction is the blue/black line while the upper and lower quartiles are the large dashed line (blue) and the 5th and 9th percentiles are the short dashed lines (blue). The median is the very large dashed line (blue). The Kp index is also plotted (purple).

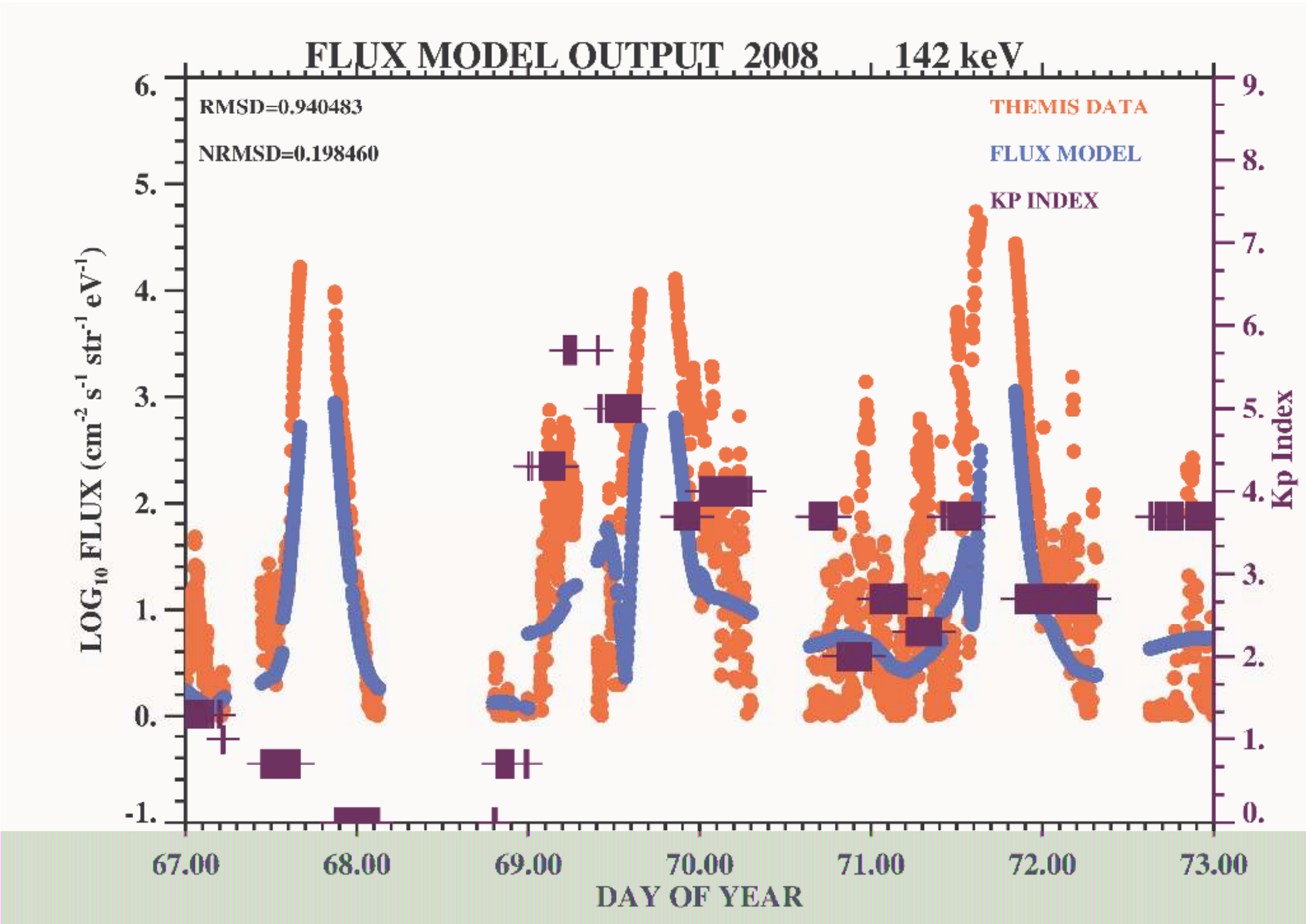

Figure 8. Comparison of in-situ electron flux values from THEMIS/SST at 142 keV (red) from DOY 67-73 in 2008 during the passage of a HSS. Conditions transition from very calm (Kp~0) to disturbed (Kp~6) Model flux predictions are plotted (blue) along with the Kp index (purple crosses, right axis).

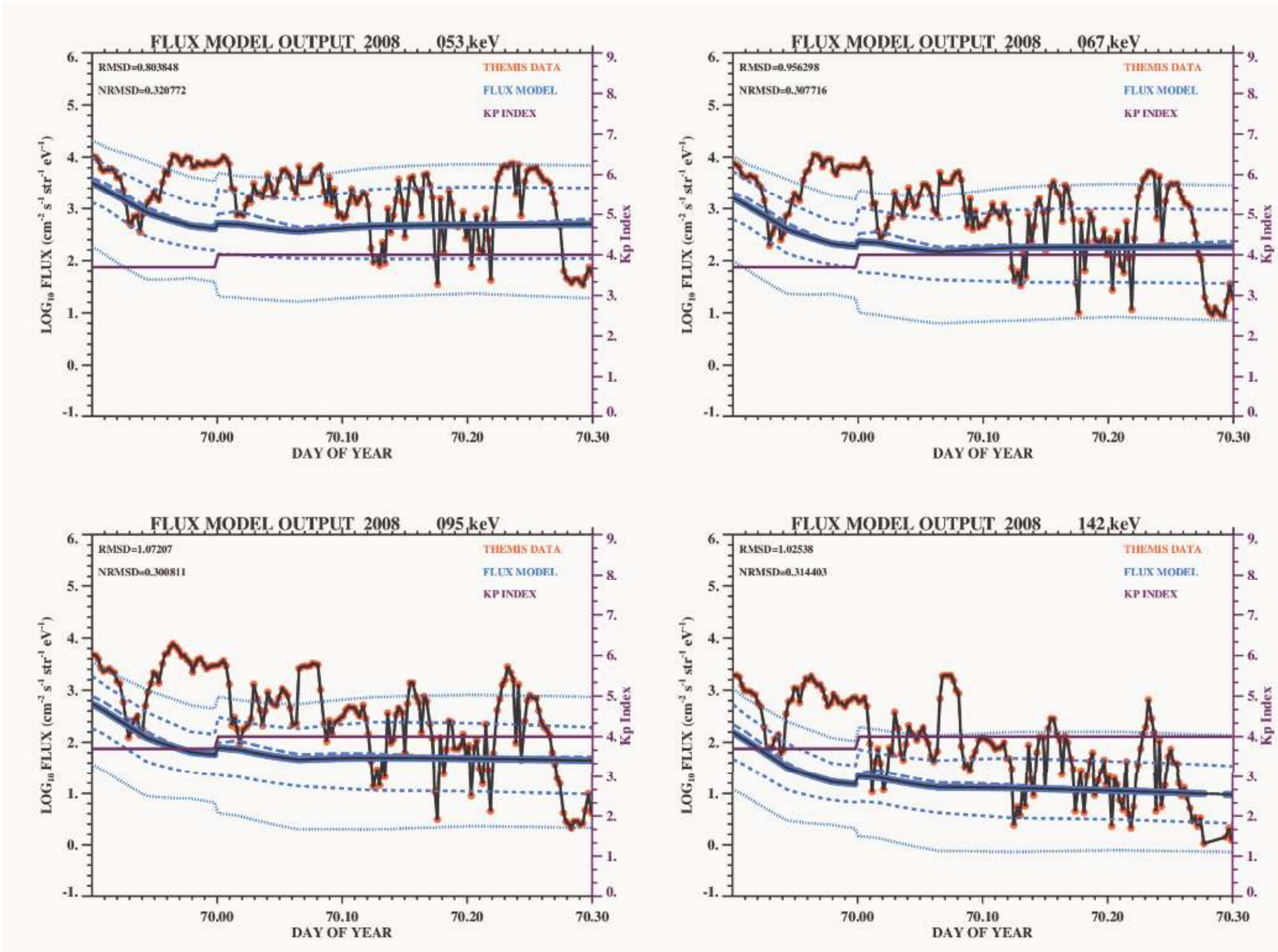

Figure 9. A detailed comparison of the observed electron fluxes (red/black) at four energies during DOY 69-70 (9-10th March) in 2008 with model flux predictions (blue). During this interval the THEMIS orbital perigee was on the nightside in the post-dusk sector (~21 LT). The mean flux prediction is the blue/black line while the upper and lower quartiles are the large dashed line (blue) and the 5th and 9th percentiles are the short dashed lines (blue). The median is the very large dashed line (blue). The Kp index is also plotted (purple).

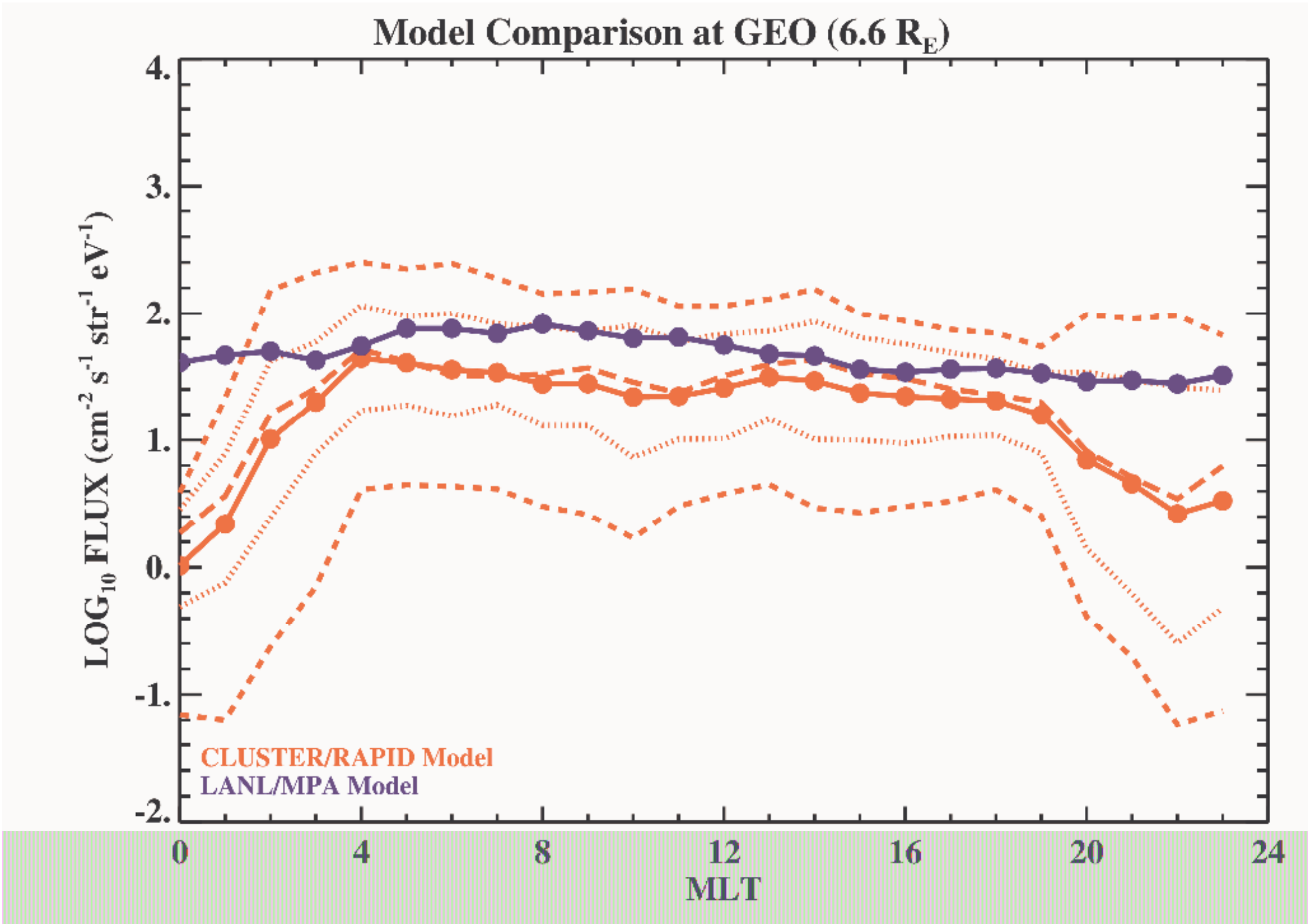

Figure 10. A comarison of the MPA flux model mean flux (thick blue line with circles) at 6.6 R_E and the new CLUSTER/RAPID model mean flux (thick red line with circles). For the CLUSTERdata the median (large dashes), upper and lower quartiles (short dashes) and 5th and 95th percentiles (medium dashes) are also plotted.